Available online at www.CivileJournal.org

Civil Engineering Journal

(E-ISSN: 2476-3055; ISSN: 2676-6957)

Vol. 10, No. 02, February, 2024

Effects of GFRP Stirrup Spacing on the Behavior of Doubly GFRP-Reinforced Concrete Beams

Musa AbdulMuttalib Issa [1*], Abbas A. Allawi [1], Nazar Oukaili [1]

[1] *Department of Civil Engineering, College of Engineering, University of Baghdad, Baghdad, Iraq.*

Received 14 October 2023; Revised 04 January 2024; Accepted 11 January 2024; Published 01 February 2024

Abstract

This study investigates the impact of varying glass fiber-reinforced polymer (GFRP) stirrup spacing on the performance of doubly GFRP-reinforced concrete beams. The research focuses on assessing the behavior of GFRP-reinforced concrete beams, including load-carrying capacity, cracking, and deformability. It explores the feasibility and effectiveness of GFRP bars as an alternative to traditional steel reinforcement in concrete structures. Six concrete beams with a cross-section of 300 mm (wide) × 250 mm (deep), simply supported on a 2100 mm span, were tested. The beams underwent four-point bending with two concentrated loads applied symmetrically at one-third of the span length, resulting in a shear span (a)-to-depth (h) ratio of 2.8. The experimental findings reveal that altering the GFRP stirrup spacing along the longitudinal axis of the beams, from 200 mm (equivalent to the effective depth (d)) to 50 mm (equal to (d⁄4)), altered the mode of failure from flexure-shear to flexure-compression. However, when the spacing was equal to or less than (d⁄3), there was no significant improvement in load-carrying capacity, as the contribution of GFRP bars in resisting shear loads was limited. Under service loads, the GFRP-reinforced beams exhibited wider cracks, but reducing the stirrup spacing helped restrain crack widening. Incorporating GFRP bars in the compression zone had a positive effect on reducing crack width in the tension zone. Additionally, using GFRP stirrups with spacing varying between (d) and (d⁄2) in the pure bending region increased the deflection ductility indexes. To enhance the ductility of GFRP-reinforced concrete beams, it is recommended to use GFRP stirrups in the pure bending region with spacing greater than the spacing between GFRP stirrups in the shear spans. The study highlights that the current ACI code overestimates the shear capacity provided by GFRP stirrups, particularly when the spacing is less than or equal to (d⁄3).

Keywords: GFRP Bars; Doubly Reinforced Concrete Section; Flexural Strength; Shear Strength; Dowel Action; Deflection; Cracking.

1. Introduction

A common problem that structural engineers deal with is the quick deterioration of steel bars as a result of corrosion, which shortens the lifespan of reinforced concrete structures. Thus, using FRP bars provides a way to improve the durability of structures and postpone their deterioration. Fiber-reinforced polymer (FRP) bars have become widely known as an affordable reinforcement method to address the corrosion issues that steel bars encounter in challenging conditions. Glass fiber-reinforced polymer (GFRP) bars offer an alternative approach to mitigating the problems related to the corrosion of steel bars in structural concrete members [1].

Due to its wide availability and affordable price, GFRP, a composite material characterized by a polymer matrix reinforced with glass fibers, prominently features GFRP bars [2]. With its many advantages over conventional building materials like steel, glass fiber reinforced polymer (GFRP) is a suitable option for a variety of civil infrastructure applications, including bridges, parking, and marine structures. The high strength-to-weight ratio, light weight

* Corresponding author: musa.abd2101m@coeng.uobaghdad.edu.iq

http://dx.doi.org/10.28991/CEJ-2024-010-02-011

composition, and corrosion resistance of GFRP bars are noteworthy characteristics [3–10]. However, when compared to conventional steel, GFRP reinforced bars exhibit certain drawbacks, including a relatively lower elasticity modulus, reduced ductility, and diminished stiffness. Moreover, the brittle failure tendencies of GFRP-reinforced composite elements present a major obstacle to substituting steel bars with GFRP alternatives [11]. When compared to conventional steel-reinforced concrete members, GFRP-reinforced concrete members exhibit increased crack width and deformability at different load levels due to the differentiable bonding behavior, anisotropy, and decreased stiffness of the GFRP bars [12, 13]. As a result of these substantial issues, the structural designs of such mmbers may encounter significant limitations [14].

The behavior of GFRP-reinforced concrete beams subjected to static loads has been the subject of numerous studies [15–23]. The development of design guidelines and codes for fiber-reinforced polymer structures has resulted from extensive research endeavors. These guidelines include publications like "Guide for the Design and Construction of Structural Concrete Reinforced with Fiber-Reinforced Polymer (FRP) Bars" (ACI 440.1R-15) [24] and "Design and Construction of Building Structures with Fibre-Reinforced Polymers" (CSA S806-12 (R2021)) [25]. Recent developments include specific codes for glass fiber-reinforced polymer bars, such as "Building Code Requirements for Structural Concrete Reinforced with Glass Fiber-Reinforced Polymer (GFRP) Bars-Code and Commentary" (ACI CODE-440.11-22) [26]. Under flexure, the design guidelines for GFRP-reinforced concrete members were intended to be similar to those for steel-reinforced concrete members. Empirical data from concrete members reinforced with FRP bars indicate that flexural capacity can be estimated using assumptions similar to those employed for steel-reinforced concrete members [24]. While steel-reinforced concrete sections are typically designed to exhibit tension-controlled behavior through steel yielding prior to concrete crushing, the flexural behavior of GFRP-reinforced concrete beams deviates due to the linear elastic-brittle nature of GFRP bars. This fact highlights the necessity to reevaluate the recommended tension-controlled approach for concrete sections. Instead, compression-controlled behavior is a somewhat preferred approach for flexural members reinforced with GFRP bars. The occurrence of concrete crushing before GFRP reinforcement tensile rupture introduces a degree of inelastic behavior prior to failure [24-26]. Consequently, over-reinforcement of GFRP-reinforced concrete beams is advised in design to ensure failure happens through concrete crushing rather than bar rupture, which could lead to catastrophic outcomes. Despite concrete crushing's classification as brittle failure, it remains preferable for GFRP RC flexural members. To accommodate the lack of ductility, the safety margin for designing FRP RC flexural members is greater than that for steel RC flexural members [24].

The ACI CODE-440.11-22 [26] determines the governing limit state by comparing the GFRP reinforcement ratio ρ_f to the GFRP balanced reinforcement ratio ρ_{fb}, where ρ_{fb} predicted assuming that the strain in the extreme concrete compression fibers attains the crushing value of 0.3% at the same time when the GFRP attains the design rupture strain ε_{fu}. To fulfill serviceability requirements, Vijay and GangaRao [27] advocate for ρ_f in GFRP-reinforced concrete members to exceed 1.4 times ρ_{fb}. Conversely, Xue et al. [23], proposed an upper bound of ρ_f=1.5 times ρ_{fb} for flexural members situated in the transition zone. This determination arises from a statistical analysis involving 173 flexural tests on GFRP-reinforced concrete beams, collected from various research sources.

Exclusively in the direction of their reinforcing fibers, GFRP bars possess high tensile strength, which influences their shear strength, dowel action, and bonding performance. As a result, even though the design procedures are comparable, the shear strength and development length design equations adopted by ACI 318 19 [28] differ from those used for steel reinforcement [26]. The shear strength of GFRP-reinforced concrete beams is strongly influenced by the dowel action of GFRP bars. It is believed that the dowel action contribution is smaller than that of an equivalent steel area because of the reduced strength and stiffness of GFRP bars in the transverse direction [26, 29]. Furthermore, GFRP-RC beams exhibit substantially lower shear capacity as compared to conventional RC beams. This may be explained by wider cracks breaking the interlocking mechanism between aggregaters in GFRP-reinforced concrete beams.

Because of the decreased axial stiffness $E_f A_f$ of the GFRP bars, a cross-section with GFRP flexural reinforcement has a smaller depth to the neutral axis after cracking than a steel-reinforced concrete section with similar amounts of longitudinal reinforcement [26]. In other words, the cross-section's compression zone is smaller and the crack widths are wider [30]. On the other hand, elevating the elastic modulus of GFRP bars notably enhances the shear resistance of these beams [31]. Johnson [32] evaluated GFRP reinforcement's suitability for concrete structures as shear reinforcement. Based on his research findings, GFRP stirrups exceeded the minimum design limits in terms of strength. The increased stirrup strength led to beam strengths that were greater than estimated values derived from code design specifications. However, introducing transverse shear strength via GFRP stirrups introduces increased complexity to shear design. Two main reasons for the complexity are as follows: first, because of production-related problems, the strength of hooked bars at bend points is much lower than that of equivalent straight bars; and second, because GFRP stirrups require substantial transverse strains to fail, shear designs that use GFRP transverse reinforcement frequently have an impact on limiting strains within the stirrup.

Shear failure modes of members with GFRP shear reinforcement can be classified into two types: shear-tension failure mode (controlled by the rupture of GFRP shear reinforcement) and shear-compression failure mode (controlled

by the crushing of the concrete web). The first mode is more brittle, and the latter results in larger deflections. Experimental results have shown that the modes of failure depend on the GFRP shear reinforcement index ($\rho_{fv}E_f$), where ρ_{fv} is the ratio of GFRP shear reinforcement ($\rho_{fv} = A_{fv}/b_w\, s$). As the GFRP shear reinforcement index increases, the shear capacity in shear tension increases, and the mode of failure changes from shear-tension to shear-compression [33]. In addition, the GFRP shear reinforcement index and the bond characteristics of the GFRP stirrups have a combined effect on the shear crack width, with increased reinforcement index and higher bond strengths leading to better control of shear crack widths [34].

The maximum stress that a GFRP stirrup bar can withstand due to the strength loss caused by the bend at the corners of the bar; the maximum size of diagonal cracks at the ultimate state that would not significantly reduce shear transfer by aggregate interlock; and the allowable size of diagonal cracks under service load determine the permissible stress level in GFRP shear reinforcement [26]. GFRP-reinforced concrete members can thus achieve the 0.005 limit on level of strain without prematurly jeoparadizing shear capacity due to aggregate interlock loss, and by limiting the strain in the stirrups at ultimate, crack widths under service loads can be controlled also [26]. The performance of concrete beams reinforced with different ratios of GFRP bars (0.24, 0.36, 0.48, 0.72, or 0.96%) and two concrete strengths (30 or 50 MPa) was the subject of Shin et al.'s [35] investigation. Their investigation revealed that the GFRP-reinforced beam behaved bilinearly-elastic up to failure. Unlike conventional steel-reinforced concrete beams, the stiffness of GFRP-reinforced beams is dramatically reduced after the crack appearance. Shin et al. reported that to ensure deflection is safe for serviceability requirements, members should adopt over-reinforced sections to achieve adequate stiffness for flexural design.

The sudden loss of flexural stiffness experienced by the GFRP-reinforced concrete beams following the cracking of concrete has a substantial impact on the post-cracking performance and deformability [36, 37]. The sudden loss of concrete stiffness can be attributed to the low elastic modulus of GFRP bars [36-40]. High-strength concrete optimizes the utilization of the high-strength properties of GFRP bars and improves the flexural stiffness of the cracked sections. However, it may reduce the member's overall deformability due to its lower brittleness compared to normal-strength concrete [41]. According to studies by Adam et al. [42] and Elgabbas et al. [43], GFRP-reinforced concrete beams' flexural behaviors can be greatly improved by increasing the concrete's compressive strength and the GFRP-reinforcement ratio. This is because it can lessen the beams' deformability and the width of their cracks. Despite extensive research on the use of GFRP bars as tension reinforcement in RC members, only a small number of studies have documented the effect of compression GFRP bars on the flexural behavior of beams [3, 44].

Compared to its tensile strength and modulus of elasticity, the compressive strength and modulus of elasticity of FRP reinforcement are much lower and more variable, in which the compressive to tensile elasticity modulus, and compressive to tensile strength ratios are 80% and 55%, respectively [44]. Therefore, in designing calculations, the strength of any FRP bar under compression should be disregarded [24-26]. However, it is sometimes unavoidable to place FRP bars in the compression zone of concrete flexural members. These can be seen, for instance, where the stirrups are held in position by longitudinal bars or at the support sections of continuous beams. In these situations, confinement of the FRP bars in compression zones have to be taken into account in order to avoid their instability and minimize the impact of some types of FRP bars' relatively large lateral buckling. Accordingly, the transverse FRP reinforcement in the form of ties should have a spacing smaller than the least cross-sectional dimension, 16 times the longitudinal bar diameters, or 48 times the tie bar diameters [24].

There is a lack of comprehensive assessment about the impact of compressive fiber reinforced polymer bars on the flexural strength, crack propagation, and ductility of beams, necessitating additional research. Unfortunately, the design codes and guidelines for FRP bars that are currently available (CSA S806-12 [25]; ACI 440.1R15 [24]; ACI CODE-440.11-22 [26]) have not come to a consensus on considering the contribution of compressive FRP reinforcements, particularly concerning strength, deformability, and cracking resistance. Accordingly, the main goal of this investigation is to shed more light on the controversy around the previously mentioned concern to get a better understanding by examining the overall performance of GFRP-reinforced concrete beams under monotonic static loading at various loading stages. This includes the impact of GFRP bars as compressive reinforcement on deformability, ductility, cracking, and failure load of concrete flexural members.

2. Experimental Program and Methodology

2.1. Test Specimens

The experimental design was created to explore the impact of GFRP-stirrup spacing and the existence of longitudinal GFRP bars in the compression zone on the load-carrying capacity and performance of GFRP-reinforced concrete beams. Six concrete beams were fabricated, cast, and tested in which GFRP bars were used in both longitudinal and transverse directions. All tested beams had an overall length of 2400 mm, effective loading span (l) of 2100 mm, and rectangular cross-section of 300 mm (wide) × 250 mm (deep). The beams underwent four-point bending with two concentrated loads applied symmetrically at one-third of the span length, resulting in a shear span (a)-to- overall depth (h) ratio of 2.8 (i.e., achieving constant shear span (a) of 700 mm).

GFRP bars of similar diameter were chosen for the section's tension and compression zones to mitigate the possible effects of bar size on the strength and deformation of bars and, in turn, on the response of the tested beam. Four GFRP bars with a diameter of 15.2 mm were used as the main reinforcement in tension and compression zones in all tested beams, with the exception of the reference beam R-1, where the four GFRP compression bars were replaced by two steel bars each of 8 mm in diameter. The reference beam (R-1) was considered as a singly reinforced concrete beam, where the two steel bars in compression zone were utilized to secure the GFRP stirrups in the proper position. Also, closed 8 mm diameter GFRP stirrups were uniformly distributed at 100 mm intervals along R-1 axis for shear reinforcement. The five beams were regarded as doubly reinforced with GFRP bars that were able to achieve constant reinforcement ratios of ($\rho_f = 2.0\ \rho_{fb}$) and ($\rho'_f = 1.0\ \rho_{fb}$) in the tension and compression zones of the section, respectively, resulting in a constant ratio of (ρ'_f/ρ_f) that equal to 0.5.

For transverse reinforcement, closed GFRP stirrups with an 8 mm diameter were evenly positioned at different intervals along the beam axis. In the shear and pure bending spans, three beams (B-1), (B-2), and (B-3) were transversely reinforced with GFRP stirrups spaced 100, 75, and 50 mm apart, respectively. In order to investigate the impact of stirrup confinement on the behavior of compression bars in compliance with (ACI 440.1R-15) [24], ACI CODE-440.11-22 [26], and ACI code 318-19 [28], two beams (B-4) and (B-5) were reinforced with GFRP stirrups in the shear spans at a spacing of 100 and 50 mm, respectively, and at a spacing of 200 and 100 mm in the pure bending span, respectively. To ensure consistency in the testing process, a clear concrete cover of 25 mm was maintained on both the top and bottom GFRP bars of the beam's section. This measurement was taken from the outer border of the stirrups and aimed to achieve an effective depth d of 209.4 mm. Figure 1 and Table 1 display details of the tested beams.

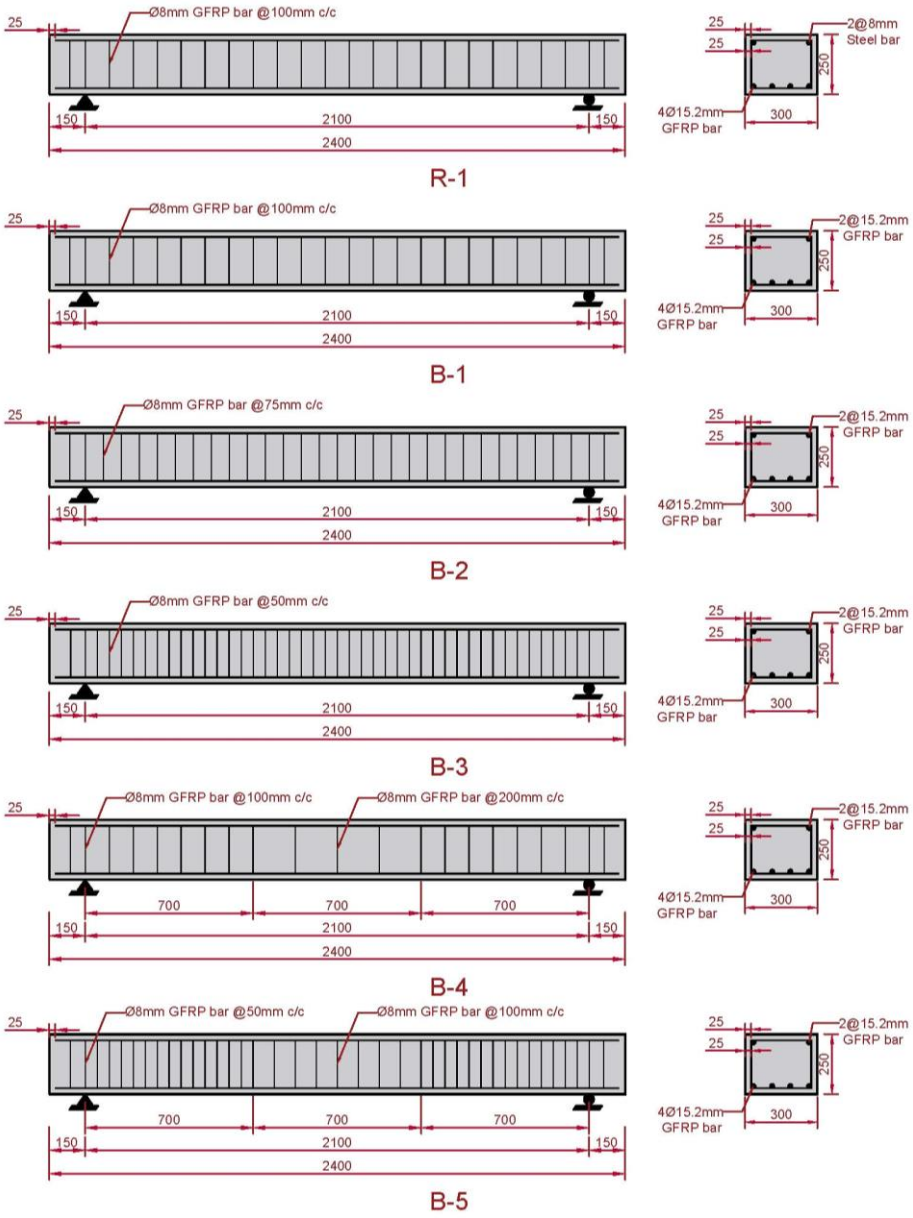

Figure 1. Details of all tested beams

Table 1. Details of longitudinal and transverse reinforcement of tested beams

Specimen ID	Stirrup spacing in shear spans s_s (mm)	Stirrup spacing in pure bending span s_m (mm)	Bars in tension zone	Bars in compression zone	$\frac{\rho'_f}{\rho_f}$
			Number, bar diameter, area, and reinforcement ratio	Number, bar diameter, area, and reinforcement ratio	
R-1	100	100	/	/	/
B-1	100	100	4Ø15.2 mm $A_f = 730.27\ mm^2$ $\rho_f = 1.16\%$ $\rho_f = 2.0\ \rho_{fb}$	2Ø15.2 mm $A'_f = 365.13\ mm^2$ $\rho'_f = 0.58\%$ $\rho'_f = 1.0\ \rho_{fb}$	0.5
B-2	75	75			
B-3	50	50			
B-4	100	200			
B-5	50	100			

2.2. Materials

2.2.1. Cement, Fine Aggregate and Coarse Aggregate

Ordinary Portland cement was used for all concrete mixes. The cement was fresh and free of lumps, with a specific gravity of 3.15. Test results confirming (ASTM-C150/C150M-17) [45].

Throughout this experiment, locally accessible graded crushed gravel with a maximum size of (19) mm was used. The specimen was prepared to yield a fairly excellent grading using 95.2% of the 20 mm passing aggregate retained on the 10 mm sieve and 31.6% of the 10 mm passing aggregate retained on the 4.75 mm sieve. The specific gravity was 2.65 and the absorption was 0.3%. For all specimens, the maximum size of the rounded-shaped natural fine aggregate particles used in the concrete mixes was 4.75 mm. The fineness modulus is 2.9. The specific gravity was 2.63 and the absorption was 1.05%. As seen in Figure 2, the sieve analysis of the combined aggregate (coarse and fine) confirm the (ASTM-C33/C33M-18) standards [46] for graded aggregate to guarantee meeting the necessary aggregate grading. Pure drinking water meeting (ASTM-C1602/C1602M-12) [47] criteria was used to make the concrete mix.

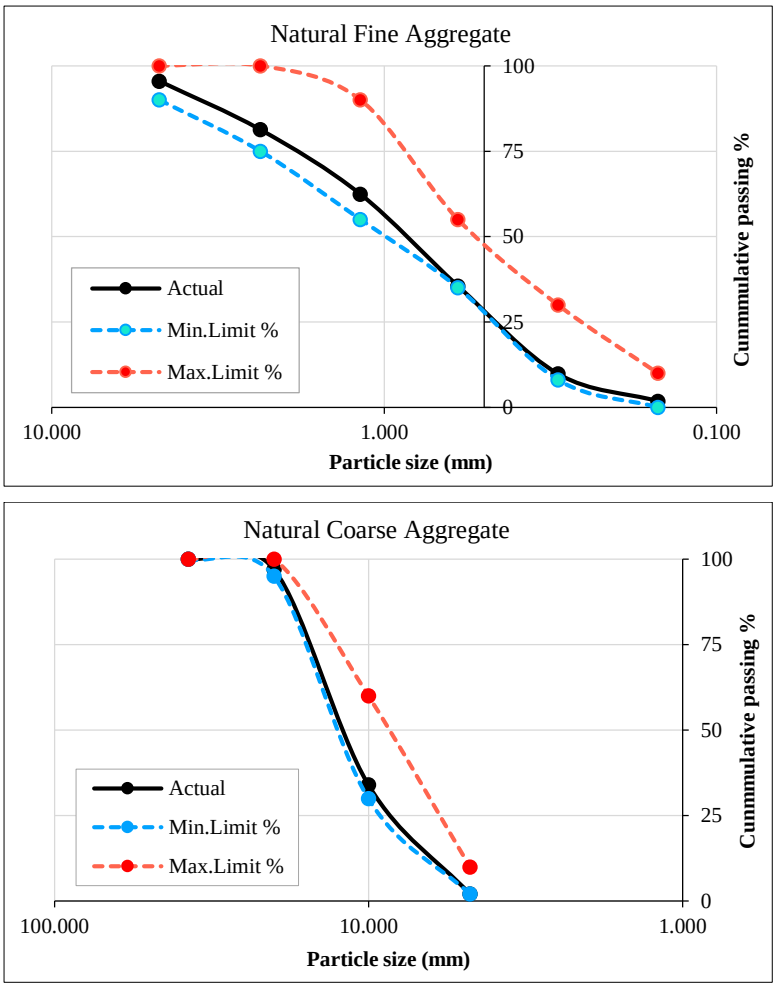

Figure 2. Sieve analysis for coarse and fine aggregate used in concrete mixes of all tested beams

2.2.2. Concrete

Different concrete mixes were developed and tested in order to reach an average target cylinder compressive strength of 48 MPa. Table 2 lists the best combination of ingredients that satisfies this requirement, including cement, sand, gravel, water, silica fume, and a specific superplasticizer admixture. ASTM C494/C494M [48]-compliant chemical additives are utilized to increase the mix's workability without sacrificing the concrete's ultimate strength. The components and their corresponding amounts needed for one cubic meter of this concrete mix are considered in Table 2.

Six 150 × 300 mm concrete mix cylinders were arbitrarily cast and tested from the same beam batches in order to preserve the mix's quality. The protocols described in ASTM C39/C39M-20 [49] and ASTM C496/C496M-17 [50] were followed in conducting these tests in order to estimate the compressive strength (f_c') and splitting tensile strength (f_t), respectively. Table 2 displays the average values for these concrete strengths.

Table 2. Mixture proportions of concrete and achieved strengths

Cement (kg/m^3)	Gravel (kg/m^3)	Sand (kg/m^3)		Water (liter/m^3)	Silica fume (kg/m^3)
470	945	827		147	20
Compressive strength f_c', (MPa)				**Splitting strength f_t, (MPa)**	
48.1	48.4	48.7	4.16	3.92	4.1
Average value 48.4				Average value 4.06	

2.2.3. GFRP Bars

The GFRP bars that were used to reinforce the tested specimens were manufactured through the pultrusion process, using thermosetting polyester resin and continuous E-glass fibers. The GFRP bars' surfaces were covered in helical glass fiber strands to improve their bonding qualities. A series of tensile tests were performed on GFRP bars of different diameters to assess their mechanical properties, such as tensile strength, ultimate strain, and modulus of elasticity. The ISO10406-1:2008 [51] standards were followed in these tests.

The high strength of GFRP bars makes testing them in direct uniaxial tension, like conventional mild steel reinforcing bars, difficult. Test results may be misleading if fibers are crushed by pressing directly onto the ends of GFRP bars under substantial forces. To solve this problem, a technique was used in which the ends of the GFRP bars were epoxy-bonded to steel couplers following ISO10406-1:2008 regulations [51].

The GFRP bars were enclosed by these steel couplers, which were made in different set lengths and diameters. These steel couplers were fabricated in various fixed lengths and diameters and were used to encase the GFRP rebars using epoxy adhesives. Because of its remarkable tensile strength, this safety measure was necessary to keep the GFRP bars from slipping during testing. Three samples of GFRP bars with diameters of 8 mm and 15.2 mm each were subjected to tensile testing, where a progressive uniaxial tensile force was applied until the tested bars failed. The possible reasons behind this failure of the test samples are either a complete rupture of the GFRP bar itself or a failure of the epoxy bond between the tested bar and the steel coupler. Table 3 contains an extensive summary of the outcomes of the tensile tests that were performed on the GFRP bars.

Table 3. Test results of GFRP bars under uniaxial tension

Specimen ID	Diameter (mm)	Area (mm^2)	Tensile strength (MPa)	Minimum specified tensile strength (MPa)	Ultimate strain (%)	Modulus of elasticity (MPa)	Minimum specified modulus of elasticity (MPa)
R-1	8	50	1875		2.80	70310	
B-1	8	50	1897	1635	2.70	74080	67517
B-2	8	50	1746		2.10	73173	
B-3	15.2	184.8	1107		2.13	51910	
B-4	15.2	180.5	1247	1000	2.32	53607	50551
B-5	15.2	182.4	1258		2.38	52656	

The minimum specified tensile strength and minimum specified modulus of elasticity shall be taken as the mean value of the test multiplied by F.

$$F = \frac{1-1.645\,\vartheta}{1+\frac{1.645\,\vartheta}{\sqrt{n}}} \quad (1)$$

where ϑ is the coefficient of variation (COV) obtained from qualification tests, and n is the number of samples = 3.

3. Theoretical Flexure and Shear Strengths of FRP-Reinforced Concrete Members

An FRP-reinforced flexural member's load capacity depends on whether it is controlled by FRP rupture or concrete crushing. In cases when the concrete is crushed (i.e., $\rho_f > \rho_{fb}$), the FRP reinforcement ratio can be used to express the nominal flexural strength of the section (M_n), as provided by Equation 2.

$$M_n = \rho_f f_f \left(1 - 0.59 \frac{\rho_f f_f}{f_c'}\right) b\, d^2 \quad (2)$$

where f_f is stress in FRP reinforcement in tension; b is width of rectangular cross section; d is distance from extreme compression fiber to centroid of tension reinforcement.

$$f_f = \left[\sqrt{\frac{(E_f\, \varepsilon_{cu})^2}{4} + \frac{0.85\, \beta_1\, f_c'}{\rho_f} E_f\, \varepsilon_{cu}} - 0.5\, E_f\, \varepsilon_{cu}\right] \leq f_{fu} \quad (3)$$

where E_f is design or guaranteed modulus of elasticity of FRP defined as mean modulus of sample of test specimens; ε_{cu} is ultimate strain in concrete; β_1 is factor taken as 0.85 for concrete strength f_c' up to and including 28 MPa. For strength above 28 MPa, this factor is reduced continuously at a rate of 0.05 per each 7 MPa of strength in excess of 28 MPa, but is not taken less than 0.65; f_{fu} is design tensile strength of FRP, defined as the guaranteed tensile strength multiplied by the environmental reduction factor.

According to ACI CODE-440.11-22 [26], the nominal one-way shear strength of a reinforced concrete cross-section, V_n, is the sum of the shear resistance provided by concrete V_c and the shear strength provided by GFRP transverse reinforcement V_f. Between the values determined by Equations 4 and 5, the shear strength offered by concrete V_c is the greater of the two.

$$V_c = 0.42\, \lambda_s\, k_{cr} \sqrt{f_c'}\, b_w\, d \quad (4)$$

$$V_c = 0.066\, \lambda_s \sqrt{f_c'}\, b_w\, d \quad (5)$$

$$\lambda_s = \sqrt{\frac{2}{1+0.004\, d}} \leq 1 \quad (6)$$

$$k_{cr} = \sqrt{2\, \rho_f\, n_f + (\rho_f\, n_f)^2} - \rho_f\, n_f \quad (7)$$

$$V_f = A_{fv}\, f_{ft} \frac{d}{s} \quad (8)$$

where λ_s is size effect factor used to modify shear strength based on the effects of member depth; k_{cr} is ratio of the depth of the elastic cracked transformed section neutral axis to the effective depth. Its value shall not be taken greater than 1, nor less than 0; b_w is web width or diameter of circular section; n_f is modular ratio ($=E_f/E_c$); A_{fv} is area of GFRP shear reinforcement within spacing s; f_{ft} is design tensile strength of GFRP transverse reinforcement that shall not exceed the smaller of the design tensile strength of bent portion of GFRP reinforcement (f_{fb}) and ($0.005\, E_f$); s is center-to-center spacing of transverse reinforcement.

Table 4 summarizes the theoretical flexure and shear strength capacities of GFRP-reinforced concrete members computed based on Equations 2-8 using test data regarding the mechanical properties of materials (concrete and GFRP bars) and the cross-sectional dimensions.

Table 4. Theoretical flexure and shear strength capacities of tested beams

Specimen ID	Stirrup spacing in shear spans s_s (mm)	Stirrup spacing in pure bending span s_m (mm)	Flexure capacity		Shear capacity	
			P_n (kN)	M_n (kN.m)	P_n (kN)	V_n (kN)
R-1	100	100	218.69	153.08	212.05	106.03
B-1	100	100			212.05	106.03
B-2	75	75			261.05	130.53
B-3	50	50			357.88	178.94
B-4	100	200			212.05	106.03
B-5	50	100			357.88	178.94

4. Test Setup and Instrumentation

Testing was conducted at the University of Baghdad's Structures laboratory utilizing a testing closed-loop rig equipped with a load control capability and a static actuator with a capacity of 150 metric tons. Four-point bending testing was performed on every beam. The stiff supports that were applied enabled the tested beams to move in both horizontal and rotational directions, simulating roller supports. Using a load control test, the specimens were subjected to a monotonically increasing load of 5 kN loading step till failure. An average of two to three hours were needed for the entire testing process, depending on the load carrying capacity and ductility of the tested beam.

The load was applied vertically at the middle of the rigid distributor steel beam, where it was eventually divided between the two bearings that were positioned 700 mm apart on top of the tested beam. Figure 3 provides a representative view of the beams during the testing process.

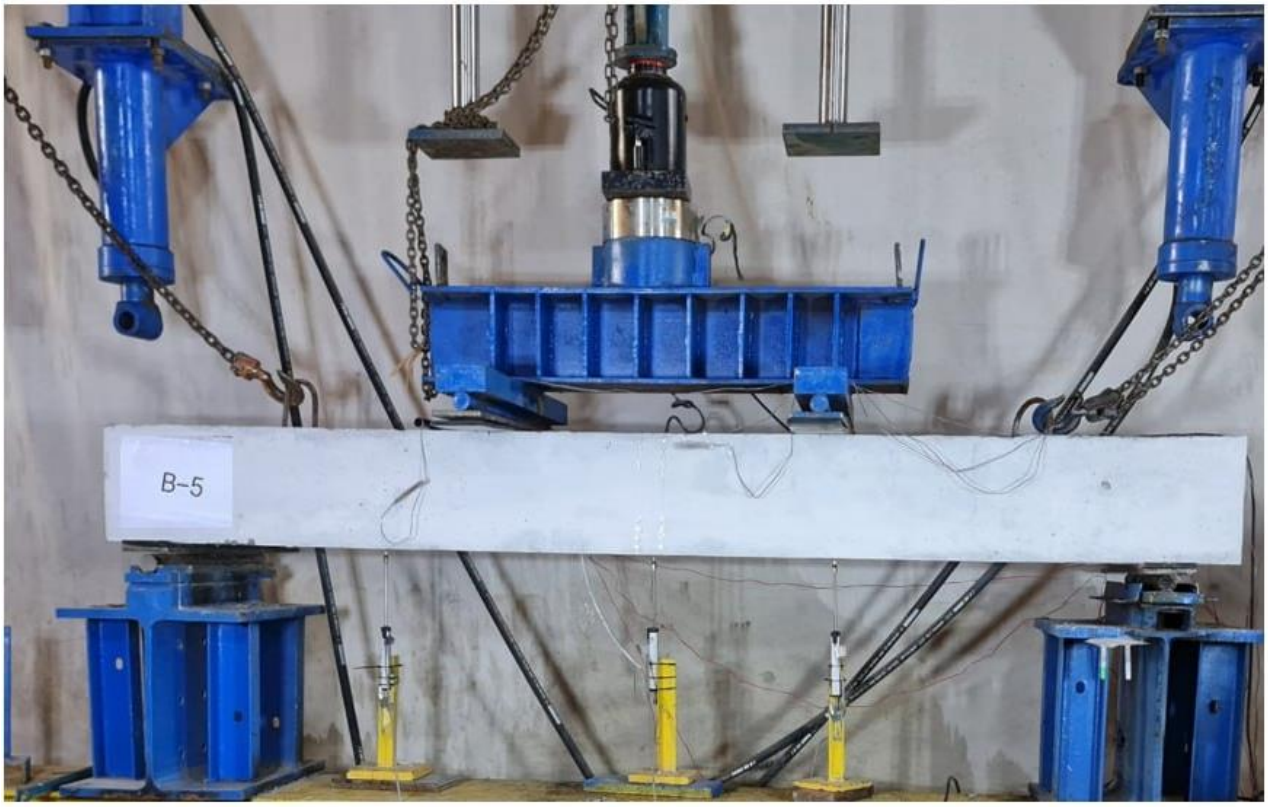

Figure 3. Typical view of the test setup

During testing, strain readings were recorded. Using prewired electrical resistance strain gauges Type UBFLA-1-5L, which have a 1 mm length and are glued to the surface of the bars in compression and tension zones, the strains in the GFRP-reinforcing bars were measured at the midspan section. Strain gauges Type PL-60-11-3LJC-F, measuring 60 mm in length, were also affixed to the extreme top and bottom fibers of the concrete at the same section. In the section situated at a distance (d) from the face of support, strain gauges of Type FLAB-3-11-3LJC-F measuring 3 mm in length were utilized on both of the GFRP stirrup's legs for steel stirrups.

Three linear voltage differential transducers (LVDTs) were used to measure the displacement of the tested beams at three separate locations: primarily at the midspan section, under one of the imposed two-point loads, and close to the left support. A microscope was utilized to track the crack width's progression. A computerized data gathering system was used to automatically monitor the strain gauge and LVDT readings during the testing. New cracks were looked for and their depth, width, and spacing were systematically inspected.

The cracks were identified using blue lines that show the crack location and the matching total applied load in (kN) that created it, see Figure 4. The test findings, which captured the behavior of the concrete beams up to the ultimate failure stage, were all recorded by a data logger and saved in the form of tables including hundreds of thousands of instantaneous data on a personal computer.

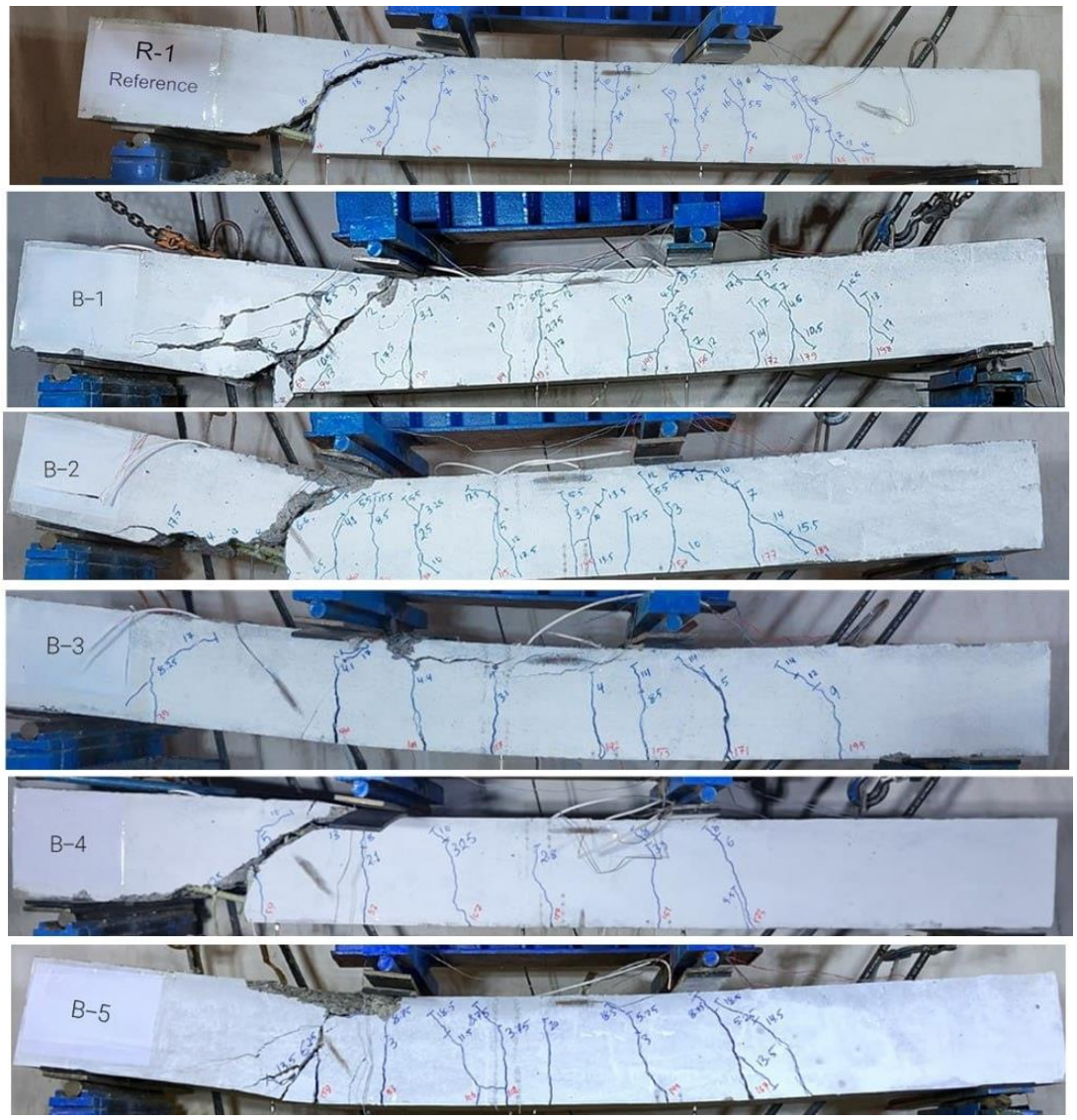

Figure 4. Crack pattern for tested beams

5. Analysis of Experimental Outcomes

5.1. Modes of Failure and Crack Pattern

All tested concrete beams reinforced with GFRP experienced initial flexural cracking near the mid-span section. It was noted that these almost vertical cracks developed randomly throughout the crack growth phase, starting from the area mainly exposed to bending force and progressively spreading outward toward the supports, including the whole tested beam. These cracks were notably scarce, spaced further apart, and of wider opening. Over time, the cracks in the beam continued to spread upward until it eventually failed during testing.

It's crucial to remember that, despite the original intention was to design these type of beams with an over-reinforced concept, the observed mode of failure in all cases was predominantly due to flexure-shear cracking. This pattern of failure that is consistent for all beams indicates that proper shear strength should be prioritized over flexural strength when designing GFRP-reinforced concrete beams.

Just before the collapse of the beams, a distinct crackling sound was heard due to the rupture of GFRP stirrups. At this stage of loading, the beam failed abruptly, resulting in a sudden drop in the applied load. Figure 4 illustrates the crack pattern observed in the tested beams, and Table 5 summarizes important parameters such as the first cracking load (P_{cr}), midspan deflection corresponding to the first cracking load (Δ_{cr}), failure load (P_u), midspan deflection corresponding to the failure load (Δ_u), and the mode of failure for all the beams that were tested. It should be noted that a high standard deviation in the failure load does not always imply a significant degree of variability in the bar's mechanical properties because the mode of failure is flexure-shear rather than tensile rupture.

Instead, the failure load was significantly influenced by the characteristics of the concrete used in the specimens.

Referring to Table 5, it's evident that the failure load of doubly GFRP-reinforced concrete beams exhibits variability compared to the singly GFRP-reinforced beam (R-1). With load capacity differences ranging from -11.07% to +13.38%,

the comparison between the reference (R-1) and other beams (B-1, B-2, B-3, B-4, and B-5) indicates an unstable nature. Due to differences in material properties, especially in the concrete, some of the doubly GFRP-reinforced beams even show lower strength than their corresponding singly CFRP-reinforced beams. It is evident that while calculating the design of GFRP-reinforced flexural members, the strength of the compression GFRP bars may be disregarded.

Table 5. Experimental outcomes of tested beams

Specimen ID	s_s (mm)	s_m (mm)	P_{cr} (kN)	Δ_{cr} (mm)	P_{ser} (kN)	P_u (kN)	Δ_u (mm)	P_{cr}/P_u (%)	P_{ser}/P_u (%)	$P_{cr}/P_{cr,R-1}$ (%)	$P_u/P_{u,R-1}$ (%)	Failure Mode
R-1	100	100	32.0	0.85	87.5	218.46	30.09	14.65	40.1			Flexure-shear
B-1	100	100	27.5	1.02	74.1	216.38	32.35	12.71	34.2	85.94	99.05	Flexure-shear
B-2	75	75	25	0.9	70.6	209.22	38.30	11.94	33.7	78.125	95.77	Flexure-shear
B-3	50	50	31	0.75	69.3	239.05	44.03	12.96	29.0	96.875	109.425	Flexure-compression
B-4	100	200	30	1.76	66.5	194.27	31.92	15.44	34.2	93.75	88.927	Flexure-shear
B-5	50	100	30	2.32	61.4	247.69	55.57	12.11	24.8	93.75	113.380	Flexure-compression

For evaluating the impact of decreasing the spacing to 75 mm and 50 mm in beam B-2 and B-3 respectively, a reference specimen, beam (B-1), with equally spaced GFRP stirrups in shear and bending moment spans of 100 mm will be utilized. As a result of this, the load capacity of specimen B-2 decreased by 3.3%, and there was a 10.5% increase in specimens (B-3). The GFRP-transversely reinforced concrete beams show an inconsistent trend of achievement for the load capacity, according to this data.

By comparing B-4 and B-1, one can eliminate the impact of the stirrups in shear spans and observe that a 10.2% reduction in load capacity results from changing the space between stirrups in pure bending span from 200 mm (in B-4) to 100 mm (in B-1). This is explained by the important function that the transverse GFRP stirrups play in preventing instability and reducing the effects of the comparatively considerable lateral buckling of some longitudinal GFRP bars in this region. On the other hand, it was found contradictory that, when comparing B-3 and B-5, where the same 50 mm stirrup spacing was used in both beams, increasing the space between stirrups in pure bending span from 50 mm (in B-3) to 100 mm (in B-5) results in a 3.6% increase in load capacity.

Nevertheless, specimen B-5 with stirrup spacing in the shear spans of 50 mm and in the pure bending span of 100 mm demonstrated a statistically significant increase in the load capacity in comparison to specimen B-4, which had doubled value stirrup spacing in the shear and pure bending spans of 100 and 200 mm, respectively. This led to a 21.6% increase in the failure load for specimen (B-5). On the other hand, the tested beams' load capacity increased and their failure mode transformed from a combination of flexure and shear to primarily flexure and compression when the GFRP stirrup spacing in shear spans reached 50 mm (i.e., = $d/4$), see Table 6.

Table 6. Comparisons of experimental and theoretical flexure and shear strengths

Specimen ID	Stirrup spacing		Experimental failure load	Theoretical flexural capacity		Theoretical shear capacity	
	in shear spans s_s (mm)	in pure bending span s_m (mm)	P_u, (kN)	P_{uf}, (kN)	P_{uf}/P_u	P_{us}, (kN)	P_{us}/P_u
R-1	$100 \approx d/2$	100	218.46	218.69	1.001	212.05	0.971
B-1	$100 \approx d/2$	100	216.38		1.011	212.05	0.980
B-2	$75 \approx d/3$	75	209.22		1.045	261.05	1.248
B-3	$50 \approx d/4$	50	239.05		0.915	357.88	1.497
B-4	$100 \approx d/2$	200	194.27		1.126	212.05	1.092
B-5	$50 \approx d/4$	100	247.69		0.883	357.88	1.445
Average					**0.997**		**1.205**
Standard of deviation (σ)					**0.088**		**0.229**
Coefficient of variation (COV)					**0.088**		**0.190**

A comparison of the theoretically estimated and experimentally measured flexural and shear strengths is given in Table 6. Analyzing Table 6's data reveals that the estimated shear capacity was almost overestimated, especially in cases where the GFRP stirrup spacing is one-third or less of the effective depth ($d/3$); the ACI CODE-440.11-22 [26] calculation methodology provided standard deviation and coefficient of variation for the ratios of the estimated shear strength to the experimental values of 0.229 and 0.190, respectively. The flexure strength of the tested beams was, nevertheless, fairly estimated by the aforementioned code; the standard deviation and coefficient of variation for the ratios of the estimated flexure strength to the experimental values were, respectively, 0.088.

5.2. Deformability of Tested Beams

Each of the three LVDTs provided the deflection data, and the midspan results were chosen to be plotted against the load measurements acquired from the load cell inside the closed-loop testing rig's jack system.

Two primary behaviors of GFRP-reinforced concrete sections are shown by the load-displacement curves for the six evaluated GFRP-reinforced concrete beams, among other significant properties. Figure 5 illustrates two distinct behaviors: (1) bilinear behavior and (2) linear-elastic behavior up to failure following the development of cracks in the concrete section. As depicted in Figure 5, the load-deflection relationship of the tested beams was linear until cracks started to appear. This was followed by two different patterns in their behavior. The low elastic modulus of the longitudinal GFRP bars caused a significant drop in stiffness during concrete cracking, resulting in a bilinear relationship. However, the structural integrity of all the tested beams was maintained since the GFRP bars did not rupture. This was demonstrated by the post-peak behaviors of all the beams in Figure 5. Table 5 illustrates that greater deformation capacity in terms of final deflection is associated with smaller stirrup spacing, and vice versa, based on a comparison of the experimental data given in Figure 5. Also, the addition of longitudinal GFRP-bars in the compression zone of the section increased the ultimate displacement capacity Δ_u of all the tested specimens, with a maximum value of 84.7% for the B-5 beam in comparison to the singly reinforced specimen R-1.

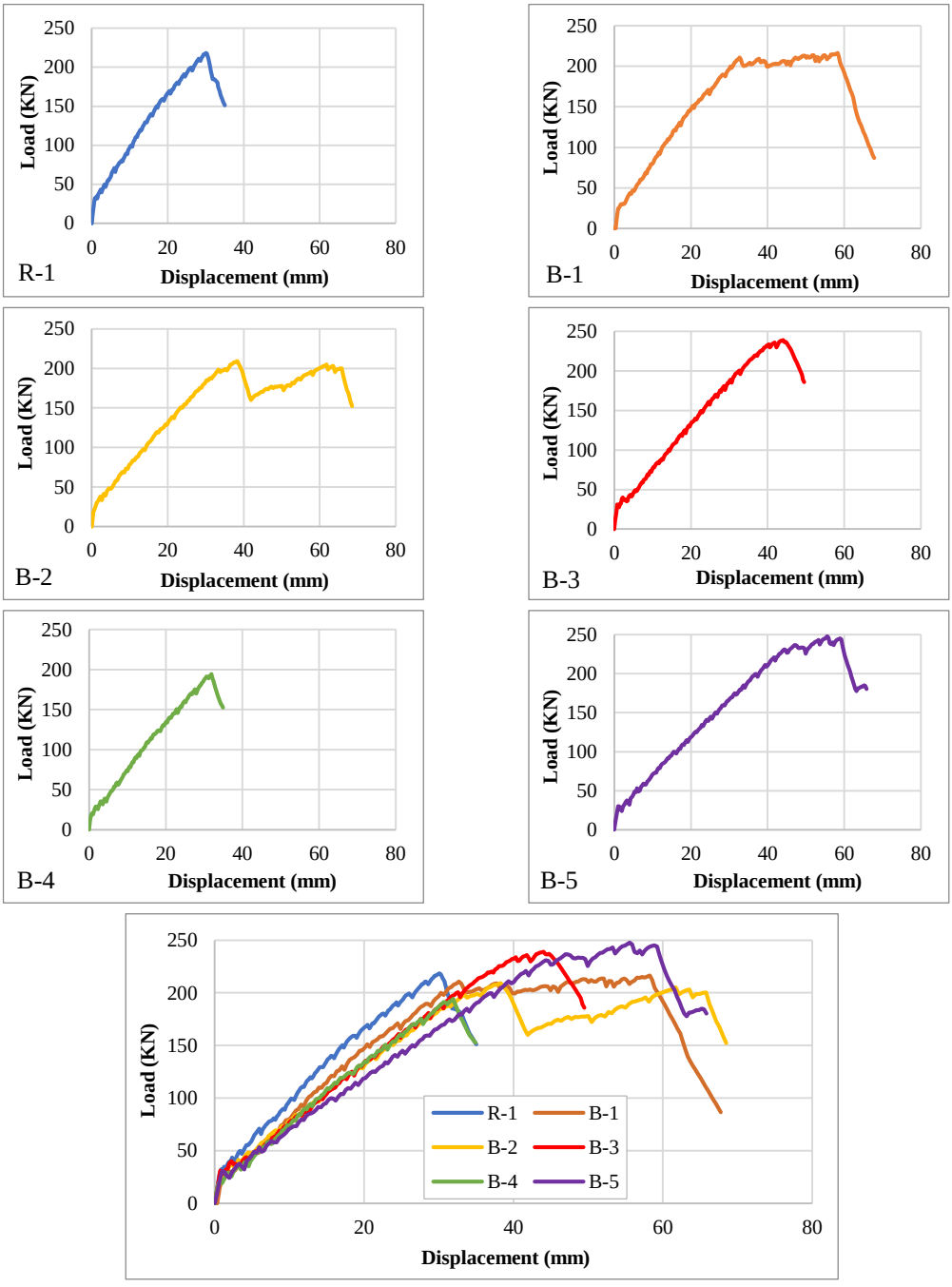

Figure 5. Load – midspan displacement plots for tested beams

The service deflection limit Δ_{ser} of $l/240$ under total service load P_{ser}, which is equal to 8.75 mm for the beams considered in this study, is specified by the ACI 440.1R-15 [24] and the ACI CODE-440.11-22 [26]. Using the experimental load-deflection data presented in Table 5, the total service load P_{ser} was calculated. It is evident that the midspan deflection Δ_{ser} of 8.75 mm corresponds to a total service load P_{ser} that ranges from 24.8% to 40.1% of the failure load. As a result, according to ACI 318-19 [28], the range of expected total service loads for GFRP-reinforced concrete flexural members is substantially smaller than the range assumed for steel-reinforced concrete members, which is normally between 60% and 70% of the ultimate load. This finding emphasizes how crucial it is to take the service load condition into account when designing GFRP-reinforced concrete flexural members.

5.3. Cracking History of Beam Specimens

When discussing the cracking process in structural concrete elements, two separate phases are typically distinguished: the first phase is known as initial crack formation, and the second phase is known as stabilized cracking. Cracks appear at random locations where the material is locally weaker during the crack formation phase. When the cracking achieves a stable condition, the applied load causes the existing cracks to spread rather than create new ones. As a result, during the stable cracking phase, the width of individual cracks keeps growing while the distance between them stays constant.

The cracking propagation at different load levels along the entire length of the beams was recorded systematically. In order to figure out the width and spacing of the cracks during loading phases, each crack along the span of the tested beam was tracked. The crack patterns seen in each tested beam are shown in Figure 4. It was observed that throughout the time of crack formation, the cracks originated in the central middle span of the beams and formed randomly, mostly in a vertical orientation. Additionally, a few wider cracks were visible. As the applied load increased, additional inclined cracks appeared due to shear forces affecting the principal tensile stresses. Because of the combined impacts of flexure and shear in cross-sections with higher bending moments, cracks in the shear span that had initially grown vertically also began to inclination. Eventually, the already-existing cracks kept becoming wider and no new ones appeared.

Figure 4 illustrates that, in tested beam, an increase in crack spacing and a decrease in the number of cracks are often associated with a decrease in stirrup spacing. The number of cracks that appeared on the beams B-1 and B-2 during loading was higher than that of beams B-3 and B-5. It is noteworthy that specimens B-1, B-2, and B-4 displayed a flexure-shear mode of failure, in which large (wide), shear (inclined) crack developed at the bottom concrete fibers near the support section and expanded toward the top concrete fibers in the vicinity of the applied load section. Meanwhile beams B-3 and B-5 exhibited a flexure-compression mode of failure, whereby horizontal cracks formed at the top concrete fibers of the beams prior to failure. In general, horizontal cracks that initiated failure at the compression zone before concrete crushing occur without additional flexural crack propagation patterns, so the influence of flexural crack formation and their propagation on the flexure-compression mode of failure of beams B-3 and B-5 was not significant. In comparison to specimens B-3, B-4, and B-5, specimens B-1 and B-2 showed a longer cracking distribution, indicating more concrete engagement in flexural capability.

Table 7 provides details on experimental observations, including the average S_{avg}, minimum S_{min}, and maximum crack spacing S_{max} at different loading stages within the central span of the beam's soffit and the number of cracks that developed at failure.

For the tested beams, the average crack spacing varied between 122 and 175 mm. The ranges for the minimum and maximum values of crack spacing were 30 to 150 mm and 200 to 270 mm, respectively. It is noteworthy that, as Table 7 shows, the loading level at which crack spacing attained a stabilized condition P_{sta} varied from 37.6% to 83.6% of the experimental failure load P_u for the doubly GFRP-reinforced beams. However, for the singly reinforced beam R-1, it was only up 36.6%.

Table 7. Experimental maximum, minimum, and average crack spacing at failure stage

Specimen ID	Stirrup spacing		Crack spacing			Number of cracks	P_u (kN)	P_{sta} (kN)	P_{sta}/P_u (%)
	s_s (mm)	s_m (mm)	S_{max} (mm)	S_{min} (mm)	S_{avg} (mm)				
R-1	100	100	250	60	130	11	218.46	80	36.6
B-1	100	100	260	40	140.9	10	216.38	170	78.6
B-2	75	75	200	30	122	11	209.22	175	83.6
B-3	50	50	250	110	175	7	239.05	90	37.6
B-4	100	200	250	150	215	7	194.27	125	64.3
B-5	50	100	270	60	150	8	247.69	145	58.5

5.4. Crack Width

The width of cracks in reinforced concrete structures is an important factor to consider when assessing the ability of steel reinforcement to withstand corrosion. However, if glass fiber reinforced polymer (GFRP) is used instead of conventional steel bars for reinforcement, the size of cracks that form in the structural concrete members has less impact on their durability [52]. During testing, the experimental crack width was carefully monitored at each load step. To achieve this, a mechanical extensometer with demic points was used, which had a gauge length of 200 mm and a high precision of 0.002 mm. The measurements were taken at the midspan section, where the pure bending moment was applied. The demic points were placed between 50 to 100 mm apart and were equally distributed across the depth of the beam section. They were attached to the lateral surface of the section.

The investigation was specifically focused on the width of three main cracks that formed initially within the beam's span due to pure bending moments. The width measurements were taken across both the depth and the soffit of the beams. These primary cracks occur at relatively low levels of steel stress and typically extend up to the neutral axis. Two different approaches were used for estimating crack widths. First, using an optical micrometer crack meter with a precision of 0.025 mm. Second, crack widths were measured utilizing a mechanical extensometer with a 50 mm gauge length and an accuracy of 0.002 mm. The gauge had been installed in position once cracks had developed.

It was found that the flexural cracks formed under the load locations showed either smaller spacing or larger widening in comparison to the other cracks in the pure bending span. This result was attributed to a likely increase in strain and curvature in these regions. The first crack's opening width evolution is depicted in Figure 6. The results of these investigations show that, under the same applied loads, GFRP-reinforced beams frequently have a greater crack width than steel-reinforced beams because of the low elastic modulus of GFRP bars [41].

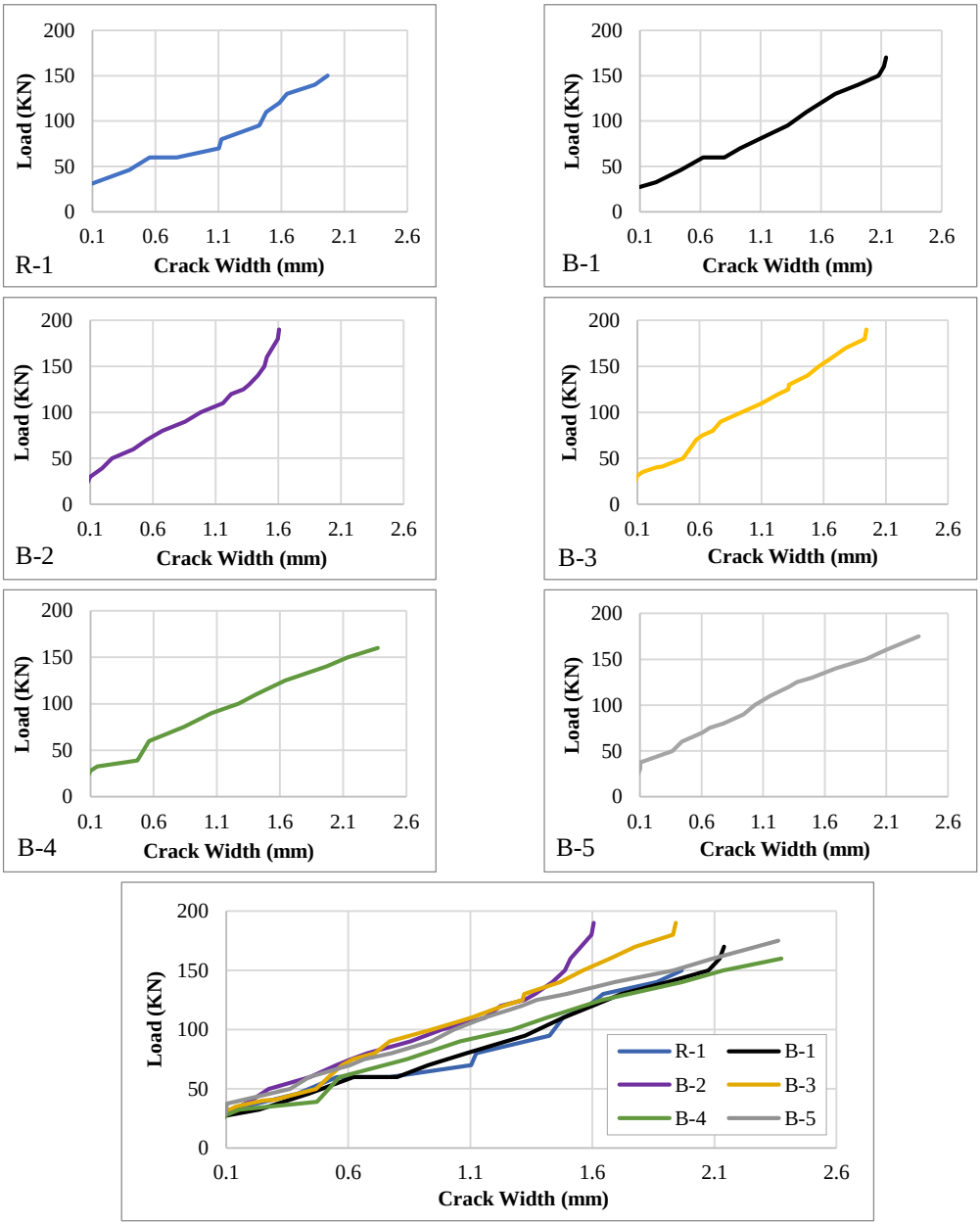

Figure 6. Progress of crack width for tested beams

Based on Figure 6, it may be concluded that when the stirrup spacing decreases, the crack width decreases as well under service load. This fact demonstrates that the shear reinforcement ratio significantly influences the crack width.

The durability of concrete structures reinforced with GFRP bars is not significantly impacted by the width of the concrete crack, in contrast to concrete structures reinforced with steel bars. Concrete members reinforced with GFRP bars in flexure may display excessive cracking for the performance of structures in service because they have much lower stiffness qualities than members reinforced with steel bars. Therefore, the concrete crack width in a GFRP-reinforced beam continues to be a major problem from the standpoint of aesthetics, serviceability requirements, and overall performance [44].

For the GFRP-reinforced concrete flexural members, it is generally acceptable to restrict crack widths in the range of 0.4 mm to 0.7 mm when crack widths are controlled for aesthetic reasons [24-26]. Nonetheless, in accordance with ACI 318-19 [28], the steel-reinforced concrete beam's crack width is often restricted to 0.4 mm. The resulting service loads $P_{0.4}$ and $P_{0.7}$ for each tested beam at which the maximum crack widths were obtained are summarized in Table 8 at 0.4 mm and 0.7 mm, respectively.

For the tested beams, a service load of 27.7 to 39.2% for doubly GFRP-reinforced concrete beams and 27.5% for singly GFRP-reinforced concrete beams resulted in a maximum crack width of 0.7 mm. In other words, if the beam design complies with serviceability requirements, the presence of GFRP bars in the compression zone improves the performance of the concrete beam by decreasing the width of the cracks in the tensile zone and increasing the design values of the applied service load. In summary, the results of the crack width limits are more restrictive than the permissible limits for deflection and stresses in GFRP-reinforced concrete beams.

Table 8. Experimental load at maximum crack width equal to 0.4 mm and 0.7 mm

Specimen ID	P_u (kN)	$P_{0.4}$ (kN)	$P_{0.7}$ (kN)	$P_{0.4}/P_u$ (%)	$P_{0.7}/P_u$ (%)
R-1	218.46	46.0	60.0	21.0	27.5
B-1	216.38	46.0	60.0	21.3	27.7
B-2	209.22	58.0	82.0	27.7	39.2
B-3	239.05	46.0	79.0	19.2	33.0
B-4	194.27	38.0	68.0	19.6	35.0
B-5	247.69	55.0	76.0	22.2	30.7

5.5. Ductility Evaluation

The term ductility refers to a beam's ability to undergo inelastic deformation without losing its load-bearing capacity before failure. By this concept, deformation or energy absorption may be utilized to evaluate ductility. The ratio of ultimate deformation to deformation at yield can be used to compute ductility in the context of steel-reinforced concrete beams, when there is evident plastic deformation of the steel at yield. GFRP bars have a linear stress-strain relationship that continues until failure, which makes the traditional concept of ductility in GFRP-reinforced concrete beams incorrect. Because both concrete and GFRP reinforcement exhibit brittle behavior, flexural members that are reinforced with GFRP bars tend to suffer from a deficiency in ductility. One of the shortcomings of GFRP-reinforced concrete members is this weakness. Consequently, even small increases in ductility brought about by GFRP reinforcement are highly valuable.

There are two methods for handling the ductility evaluation that can be found in the literature, namely the energy-based method proposed by Jeong & Naaman [53] and the deformation-based method proposed by Mufti et al. [54] and Jaeger et al. [55].

The energy-based approach defines ductility as the proportion of total energy E_t to elastic energy E_e. The total energy E_t is calculated as the area under the load-deflection curve up to the failure load. While the elastic energy E_e is determined as the area of the triangle formed at failure load by unloading the beam. To quantify the ductility of steel- and FRP-reinforced concrete beams so that they can be compared, Jeong & Naaman [53] proposed the ductility index μ_{en} as:

$$\mu_{en} = \frac{0.5\ (E_t + E_e)}{E_e} \tag{9}$$

Equation 9, which is equally relevant for beams with FRP, was developed under the supposition that the concrete beams exhibit fully elastoplastic behavior. This restriction prevents it from being widely used. Also, two locations on the load-deflection curve should be identified in order to calculate the elastic energy E_e: (a) the point that corresponds to the first drop in the curve's slope, and (b) the point corresponding to the second drop in slope. However, Figure 5 shows that point (b) is not very distinct. This is because some GFRP-reinforced beams do not undergo a second drop in stiffness caused by sudden failure.

The deformation-based approach determines the ductility as the proportion of the members' ultimate state and the service state. According to Mufti et al. [54] and Jaeger et al. [55], the concrete strain at the extreme compression fiber is approximately 0.001 under service load for concrete beams with a rectangular cross-section and based on a specific type of failure mode, namely, crushing of the concrete. It is believed that this particular strain indicates the onset of concrete's inelastic deformation. This information is used to define the service state. Mufti et al. [54] and Jaeger et al. [55] proposed the ductility index μ_D as:

$$\mu_D = \frac{M_u}{M_{0.001}} \times \frac{\Delta_u}{\Delta_{0.001}} \quad (10)$$

here M_u – moment capacity at the ultimate state (failure moment); Δ_u - deflection at the ultimate state; $M_{0.001}$ - moment at a concrete strain ε_c of 0.001 at the extreme compression fiber; $\Delta_{0.001}$ – deflection at concrete strain of 0.001 at the extreme compression fiber.

According to the Canadian Highway Bridge Design Code (CSA- S16-14) [56], concrete beams reinforced with FRP bars or grids need to have ductility index μ_D of at least 4.0 for rectangular sections and 6.0 for T-sections. Consequently, the ductility index serves as an indicator for ductile behavior.

Table 9 presents the ductility indexes μ_D for tested beam specimens based on the second approach (deformation-based approach). It is noteworthy to mention that the achieved ductility index μ_D, which ranged from 5.96 to 14.38 (i.e., more than 4), indicates that all of the tested GFRP-reinforced beams display ductile behavior despite being constructed of brittle materials like concrete and GFRP bars. This may be the result of the substantial deformation capacity of these beams, which provides a significant warranty before failure.

Table 9. Ductility indexes calculated by deformation-based approach

Specimen ID	s_s (mm)	s_m (mm)	P_u (kN)	M_u (kN.m)	Δ_u (mm)	$P_{0.001}$ (kN)	$M_{0.001}$ (kN.m)	$\Delta_{0.001}$ (mm)	$\frac{M_u}{M_{0.001}}$	$\frac{\Delta_u}{\Delta_{0.001}}$	μ_D
R-1	100	100	218.46	76.46	30.09	99.04	34.66	10.46	2.21	2.88	6.35
B-1	100	100	216.38	75.73	57.89	85.23	29.83	10.22	2.54	5.66	14.38
B-2	75	75	209.22	73.23	38.30	92.82	32.49	12.62	2.25	3.03	6.84
B-3	50	50	239.05	83.67	44.03	105.86	37.05	15.17	2.26	2.90	6.55
B-4	100	200	194.27	68.00	31.92	88.18	30.86	11.81	2.20	2.70	5.96
B-5	50	100	247.69	86.69	55.57	86.61	30.31	13.23	2.86	4.20	12.01

According to the test results, the flexural stiffness of the beams that were tested increased due to the presence of compressive GFRP bars and transverse GFRP stirrups in the pure bending span. This resulted in an increase in the ductility index. The increased stiffness could be attributed to the limited lateral deformation of the compressive GFRP bar, which may have occurred due to internal bulging and lateral buckling near the maximum compressive strain of the concrete.

The test findings show a rise in the ductility indexes, particularly when the GFRP stirrup spacing inside the pure bending span is between d and $d/2$. In order to produce better ductility, it is also recommended that this stirrup spacing in pure bending span be larger than the spacing in the shear span.

6. Conclusions

The most significant conclusions can be summarized as follows:

- The study reveals that GFRP stirrup spacing equal to or less than one-third of the effective depth ($d/3$) does not significantly enhance the ultimate load capacity of doubly GFRP-reinforced concrete beams. This lack of improvement is due to the limited effectiveness of GFRP bars in resisting shear loads. However, when the GFRP stirrup spacing is precisely equal to $d/4$, it shifts the failure mode from a combination of flexure and shear to a primary mode of flexure and compression.
- The test results indicate that the ACI CODE-440.11-22 tends to overestimate the shear strength provided by GFRP shear reinforcement, particularly when the GFRP stirrup spacing is equal to or less than one-third of the effective depth ($d/3$).
- When the spacing of GFRP stirrups is less than $d/4$, the primary mode of failure is the formation of flexure-shear cracks. This consistent failure pattern across all beams leads to the conclusion that in the design of GFRP-reinforced concrete beams, shear strength plays a more crucial role than bending strength.
- The failure load of doubly GFRP-reinforced concrete beams displays variability when compared to singly GFRP-reinforced beams. In some cases, doubly GFRP-reinforced beams exhibit lower strength than their corresponding

singly GFRP-reinforced counterparts. This variance can be attributed to differences in material properties, particularly within the concrete. Consequently, it is evident that the strength of the compression GFRP bars may be disregarded in the design calculations for GFRP-reinforced flexural members.

- Clearly, the total service load associated with a midspan deflection of $l/240$ falls within a range of 24.7% to 40.0% of the failure load for GFRP-reinforced concrete flexural members. This range is significantly lower than the assumed range for steel-reinforced concrete members specified by ACI 318-19, which typically covers 60% to 70% of the ultimate load. This underscores the critical role of the service load state in ensuring the reliability of the design for GFRP-reinforced concrete flexural members.
- GFRP-reinforced beams commonly exhibit wider crack widths. When GFRP-reinforced beams are subjected to service loads, the crack width tends to decrease as the stirrup spacing is reduced. This observation underscores the significant influence of the shear reinforcement ratio on crack width in GFRP-reinforced beams..
- In concrete beam design, incorporating GFRP bars in the compression zone has a positive impact on performance. It helps reduce the width of cracks in the tensile zone, ultimately leading to an increase in the design values of service load, especially when designing beams to meet serviceability requirementsIn GFRP-reinforced concrete beams, the restriction on crack width is typically more stringent than the allowable limits for deflection and stress. Furthermore, when considering sections designed to fail due to concrete crushing, the service load that meets serviceability requirements typically falls within a range of 22% to 38% of the ultimate load. In this context, the critical factor influencing the design is the limitation on crack width and deflection.

The test results clearly show that the deflection ductility indexes experience an increase, particularly when the GFRP stirrup spacing within the pure bending span is situated between the depth (d) and one-half of the effective depth ($d/2$). Furthermore, it is recommended that this spacing be greater than the spacing in the shear zone to enhance deflection ductility.

7. Declarations

7.1. Author Contributions

Conceptualization, A.A. and M.I.; methodology, N.O.; software, M.I.; validation, A.A., M.I., and N.O.; formal analysis, M.I.; investigation, A.A.; resources, M.I.; data curation, N.O.; writing—original draft preparation, M.I. and A.A.; writing—review and editing, N.O.; visualization, M.I.; supervision, A.A. and N.O.; project administration, A.A.; funding acquisition, M.I. and N.O. All authors have read and agreed to the published version of the manuscript.

7.2. Data Availability Statement

The data presented in this study are available in the article.

7.3. Funding

The authors received no financial support for the research, authorship, and/or publication of this article.

7.4. Conflicts of Interest

The authors declare no conflict of interest.

8. References

[1] Moawad, M. S., & Fawzi, A. (2021). Performance of concrete beams partially/fully reinforced with glass fiber polymer bars. Journal of Engineering and Applied Science, 68, 38. doi:10.1186/s44147-021-00028-6.

[2] Saleh, Z., Goldston, M., Remennikov, A. M., & Sheikh, M. N. (2019). Flexural design of GFRP bar reinforced concrete beams: An appraisal of code recommendations. Journal of Building Engineering, 25. doi:10.1016/j.jobe.2019.100794.

[3] Al-Salloum, Y., Sayed, S. H., & Almusallam, T. H. (1997). Behavior of Concrete Beams Doubly Reinforced by GFRP Bars. Proceedings of the Third International Symposium on Non-Metallic (FRP) Reinforcement for Concrete Structures (FRPRCS-3), 14-16 October, 1997, Sapporo, Japan.

[4] Said, A. M. I. (2015). Evaluation of Deflection in High Strength Concrete (HSC) I-Beam Reinforced with Carbon Fiber Reinforced Polymer (CFRP) Bars. The 7th Asia Pacific Young Researchers and Graduates Symposium, 20-21 August, 2015, University of Malaya, Kuala Lumpur, Malaysia.

[5] Said, A. I., & Tuma, N. H. (2021). Numerical Modeling for Flexural Behavior of UHPC Beams Reinforced with Steel and Sand-Coated CFRP Bars. IOP Conference Series: Earth and Environmental Science, 856(1), 12003. doi:10.1088/1755-1315/856/1/012003.

[6] Said, A. I., & Abbas, O. M. (2023). Serviceability behavior of High Strength Concrete I-beams reinforced with Carbon Fiber Reinforced Polymer bars. Journal of Engineering, 19(11), 1515–1530. doi:10.31026/j.eng.2013.11.10.

[7] Ali, S. I., & Allawi, A. A. (2021). Effect of Web Stiffeners on The Flexural Behavior of Composite GFRP- Concrete Beam Under Impact Load. Journal of Engineering, 27(3), 76–92. doi:10.31026/j.eng.2021.03.06.

[8] Mohammed, S. A., & Said, A. M. I. (2022). Analysis of concrete beams reinforced by GFRP bars with varying parameters. Journal of the Mechanical Behavior of Materials, 31(1), 767–774. doi:10.1515/jmbm-2022-0068.

[9] Ali, H. H., & Said, A. M. I. (2022). Flexural behavior of concrete beams with horizontal and vertical openings reinforced by glass-fiber-reinforced polymer (GFRP) bars. Journal of the Mechanical Behavior of Materials, 31(1), 407–415. doi:10.1515/jmbm-2022-0045.

[10] Lin, X., & Zhang, Y. X. (2013). Bond-slip behaviour of FRP-reinforced concrete beams. Construction and Building Materials, 44, 110–117. doi:10.1016/j.conbuildmat.2013.03.023.

[11] Issa, M. S., Metwally, I. M., & Elzeiny, S. M. (2011). Influence of fibers on flexural behavior and ductility of concrete beams reinforced with GFRP rebars. Engineering Structures, 33(5), 1754–1763. doi:10.1016/j.engstruct.2011.02.014.

[12] Said, M., Adam, M. A., Mahmoud, A. A., & Shanour, A. S. (2016). Experimental and analytical shear evaluation of concrete beams reinforced with glass fiber reinforced polymers bars. Construction and Building Materials, 102, 574–591. doi:10.1016/j.conbuildmat.2015.10.185.

[13] Wegian, F. M., & Abdalla, H. A. (2005). Shear capacity of concrete beams reinforced with fiber reinforced polymers. Composite Structures, 71(1), 130–138. doi:10.1016/j.compstruct.2004.10.001.

[14] Chidananda, S. H., & Khadiranaikar, R. B. (2017). Flexural behaviour of concrete beams reinforced with GFRP rebars. International Journal of Advance Research, Ideas and Innovations in Technology, 3(5), 119-128.

[15] Attari, N., Amziane, S., & Chemrouk, M. (2012). Flexural strengthening of concrete beams using CFRP, GFRP and hybrid FRP sheets. Construction and Building Materials, 37, 746–757. doi:10.1016/j.conbuildmat.2012.07.052.

[16] Goldston, M., Remennikov, A., & Sheikh, M. N. (2016). Experimental investigation of the behaviour of concrete beams reinforced with GFRP bars under static and impact loading. Engineering Structures, 113, 220–232. doi:10.1016/j.engstruct.2016.01.044.

[17] Yoo, D. Y., Banthia, N., & Yoon, Y. S. (2016). Flexural behavior of ultra-high-performance fiber-reinforced concrete beams reinforced with GFRP and steel rebars. Engineering Structures, 111, 246–262. doi:10.1016/j.engstruct.2015.12.003.

[18] Alsayed, S. H. (1998). Flexural behaviour of concrete beams reinforced with GFRP bars. Cement and Concrete Composites, 20(1), 1–11. doi:10.1016/S0958-9465(97)00061-9.

[19] Kalpana, V. G., & Subramanian, K. (2011). Behavior of concrete beams reinforced with GFRP BARS. Journal of Reinforced Plastics and Composites, 30(23), 1915–1922. doi:10.1177/0731684411431119.

[20] Toutanji, H. A., & Saafi, M. (2000). Flexural behavior of concrete beams reinforced with glass fiber-reinforced polymer (GFRP) bars. ACI Structural Journal, 97(5), 712–719. doi:10.14359/8806.

[21] Gouda, O., Hassanein, A., & Galal, K. (2023). Experimental and numerical study on the crack width and deflection performance of GFRP reinforced concrete beams. Engineering Structures, 283, 115721. doi:10.1016/j.engstruct.2023.115721.

[22] Hasan, M. A., Sheehan, T., Ashour, A., & Elkezza, O. (2023). Flexural behaviour of geopolymer concrete T-Beams reinforced with GFRP bars. Structures, 49, 345–364. doi:10.1016/j.istruc.2023.01.118.

[23] Xue, W., Tan, Y., & Zeng, L. (2010). Flexural response predictions of reinforced concrete beams strengthened with prestressed CFRP plates. Composite Structures, 92(3), 612-622. doi:10.1016/j.compstruct.2009.09.036.

[24] ACI 440.1R-15. (2015). Guide for the Design and Construction of Structural Concrete Reinforced with Fiber-Reinforced Polymer (FRP) Bars. American Concrete Institute (ACI), Michigan, United States.

[25] CSA-S806-12. (2021). Design and Construction of Building Components with Fibre-Reinforced Polymers. Canadian Standards Association, Toronto, Canada.

[26] ACI CODE-440.11-22. (2022). Building Code Requirements for Structural Concrete Reinforced with Glass Fiber Reinforced Polymer (GFRP) Bars-Code and Commentary. American Concrete Institute (ACI), Michigan, United States.

[27] Vijay, P. V., & GangaRao, H. V. S. (2001). Bending behavior and deformability of glass fiber-reinforced polymer reinforced concrete members. ACI Structural Journal, 98(6), 834–842. doi:10.14359/10750.

[28] ACI 318-19. (2019). Building code requirements for structural concrete and commentary. American Concrete Institute (ACI), Michigan, United States.

[29] Karimipour, A., & Edalati, M. (2020). Shear and flexural performance of low, normal and high-strength concrete beams reinforced with longitudinal SMA, GFRP and steel rebars. Engineering Structures, 221, 0141 0296. doi:10.1016/j.engstruct.2020.111086.

[30] El-Sayed, A. K., El-Salakawy, E. F., & Benmokrane, B. (2006). Shear capacity of high-strength concrete beams reinforced with FRP bars. ACI Materials Journal, 103(3), 383. doi:10.14359/15316.

[31] Li, W., Huang, W., Fang, Y., Zhang, K., Liu, Z., & Kong, Z. (2022). Experimental and theoretical analysis on shear behavior of RC beams reinforced with GFRP stirrups. Structures, 46, 1753–1763. doi:10.1016/j.istruc.2022.10.138.

[32] Johnson, D. T. C. (2014). Investigation of glass fibre reinforced polymer (GFRP) bars as internal reinforcement for concrete structures. Ph.D. Thesis, Toronto, Canada.

[33] Shehata, E., Morphy, R., & Rizkalla, S. (2000). Fibre reinforced polymer shear reinforcement for concrete members: Behaviour and design guidelines. Canadian Journal of Civil Engineering, 27(5), 859–872. doi:10.1139/l00-004.

[34] Ahmed, E. A., El-Salakawy, E. F., & Benmokrane, B. (2010). Fibre-reinforced polymer composite shear reinforcement: performance evaluation in concrete beams and code prediction. Canadian Journal of Civil Engineering, 37(8), 1057–1070. doi:10.1139/l10-046.

[35] Shin, S., Seo, D., & Han, B. (2009). Performance of concrete beams reinforced with GFRP bars. Journal of Asian Architecture and Building Engineering, 8(1), 197–204. doi:10.3130/jaabe.8.197.

[36] Bischoff, P. H., & Gross, S. P. (2011). Design Approach for Calculating Deflection of FRP-Reinforced Concrete. Journal of Composites for Construction, 15(4), 490–499. doi:10.1061/(asce)cc.1943-5614.0000195.

[37] Bischoff, P. H., & Gross, S. P. (2011). Equivalent Moment of Inertia Based on Integration of Curvature. Journal of Composites for Construction, 15(3), 263–273. doi:10.1061/(asce)cc.1943-5614.0000164.

[38] Mousavi, S. R., & Esfahani, M. R. (2012). Effective Moment of Inertia Prediction of FRP-Reinforced Concrete Beams Based on Experimental Results. Journal of Composites for Construction, 16(5), 490–498. doi:10.1061/(asce)cc.1943-5614.0000284.

[39] Ramachandra Murthy, A., Pukazhendhi, D. M., Vishnuvardhan, S., Saravanan, M., & Gandhi, P. (2020). Performance of concrete beams reinforced with GFRP bars under monotonic loading. Structures, 27, 1274–1288. doi:10.1016/j.istruc.2020.07.020.

[40] Chellapandian, M., Mani, A., & Suriya Prakash, S. (2020). Effect of macro-synthetic structural fibers on the flexural behavior of concrete beams reinforced with different ratios of GFRP bars. Composite Structures, 254. doi:10.1016/j.compstruct.2020.112790.

[41] Guadagnini, M., Pilakoutas, K., & Waldron, P. (2003). Shear performance of FRP reinforced concrete beams. Journal of Reinforced Plastics and Composites, 22(15), 1389–1407. doi:10.1177/073168403035579.

[42] Adam, M. A., Said, M., Mahmoud, A. A., & Shanour, A. S. (2015). Analytical and experimental flexural behavior of concrete beams reinforced with glass fiber reinforced polymers bars. Construction and Building Materials, 84, 354–366. doi:10.1016/j.conbuildmat.2015.03.057.

[43] Elgabbas, F., Ahmed, E. A., & Benmokrane, B. (2017). Flexural Behavior of Concrete Beams Reinforced with Ribbed Basalt-FRP Bars under Static Loads. Journal of Composites for Construction, 21(3), 04016098. doi:10.1061/(asce)cc.1943-5614.0000752.

[44] Hassanpour, S., Khaloo, A., Aliasghar-Mamaghani, M., & Khaloo, H. (2022). Effect of Compressive Glass Fiber-Reinforced Polymer Bars on Flexural Performance of Reinforced Concrete Beams. ACI Structural Journal, 119(6), 5–18. doi:10.14359/51734792.

[45] ASTM-C150/C150M-18. (2019). Standard Specification for Portland Cement. ASTM International, Pennsylvania, United States. doi:10.1520/C0150_C0150M-18.

[46] ASTM C33/C33M-18. (2003). Standard Specification for Concrete Aggregates. ASTM International, Pennsylvania, United States. doi:10.1520/C0033_C0033M-18.

[47] ASTM C1602/C1602M-12. (2019). Standard Specification for Mixing Water Used in the Production of Hydraulic Cement Concrete. ASTM International, Pennsylvania, United States. doi:10.1520/C0033_C0033M-18.

[48] ASTM C494/C494M. (2022). Standard Specification for Chemical Admixtures for Concrete. ASTM International, Pennsylvania, United States. doi:10.1520/C0494_C0494M-19.

[49] ASTM C39/C39M-20. (2020). Standard Test Method for Compressive Strength of Cylindrical Concrete Specimens. ASTM International, Pennsylvania, United States. doi:10.1520/C0039_C0039M-20.

[50] ASTM C496/C496M-17. (2017). Standard Test Method for Splitting Tensile Strength of Cylindrical Concrete Specimens. ASTM International, Pennsylvania, United States. doi:10.1520/C0496_C0496M-17.

[51] ISO 10406-1:2015. (2015). Fiber-reinforced polymer (FRP) reinforcement of concrete - Test methods - Part 1: FRP bars and grids. International Organization for Standardization (ISO), Geneva, Switzerland.

[52] Abdallah, W., Farrag, A. M., Deifalla, A. F., Ibrahim, A. H., Mohamed, H. M., & Ali, A. H. (2023). Shear Performance of GFRP Reinforced Concrete Beams with Seawater and Chopped Fiber. Civil Engineering Journal, 9(4), 835–848. doi:10.28991/CEJ-2023-09-04-05.

[53] Jeong, S. M., & Naaman, A. E. (1995). Ductility of concrete beams prestressed with FRP tendons. Structures Congress - Proceedings, CRC Press, 2, 1466–1469.

[54] Mufti, A. A., Newhook, J. P., & Tadros, G. (1996). Deformability versus ductility in concrete beams with FRP reinforcement. Proceedings of the 2nd International Conference on Advanced Composite Materials in Bridges and Structures, ACMBS-II, 11-14 August, 1996, Quebec, Canada.

[55] Jaeger, GL., Tadros, G., and M. A. (1995). The concept of the overall performance factor in 739 rectangular-section reinforced concrete beams. Proceedings of the Second International RILEM Symposium, 23-25 August, 1995, Ghent, Belgium.

[56] CSA- S16-14. (2017). Canadian Highway Bridge Design Code. Canadian Standards Association, Toronto, Canada.